Biomacromolecules

pubs.acs.org/Biomac

Article

High Internal Phase Emulsion-Templated Hydrophilic Polyphosphoester Scaffolds: Tailoring the Porosity and Degradation for Soft Tissue Engineering

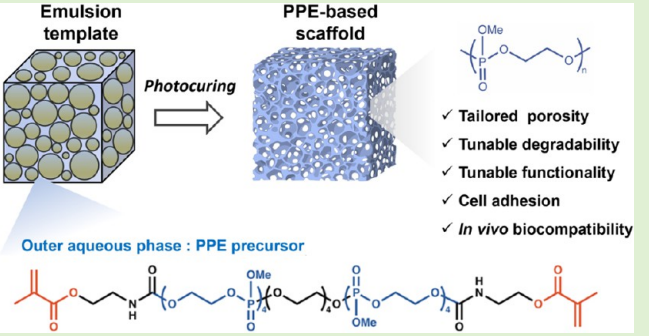
Pascal Boucq, Bernard Ucakar, Floriane Debuisson, Raphael Riva, Anne des Rieux,* Christine Jérôme,* and Antoine Debuigne*

Cite This: *Biomacromolecules* 2025, 26, 1935−1947

Read Online

ACCESS | Metrics & More | Article Recommendations | Supporting Information

ABSTRACT: Synthetic porous scaffolds are key elements in tissue engineering (TE), requiring controlled porosity for cell colonization, along with a degradation rate aligned with tissue growth. While biodegradable polyester scaffolds are widely used in TE, they are primarily hydrophobic and suited for semirigid to hard tissue applications. This work broadens the scope of TE by introducing porous scaffolds made of polyphosphoesters (PPEs), degradable polymers with adaptable physicochemical properties. PPE hydrogels were shaped into 3D scaffolds using an emulsion templating method, yielding hydrophilic matrices with controlled porosity and tunable Young's moduli for soft tissues. Degradation assays at physiological pH confirmed the scaffolds' biodegradability. Cytotoxicity tests with PPE scaffolds showed excellent cell viability, while RGD functionalization further enhanced cell adhesion. Scaffold colonization, low inflammation, and angiogenesis were demonstrated *in vivo* through subcutaneous implantation of the scaffolds in mice and histological analysis. These results highlight PPE-based scaffolds as promising candidates for regenerative medicine.

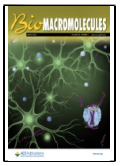


1. INTRODUCTION

Three-dimensional porous scaffolds are a key element of tissue engineering and regenerative medicine whether for an *in vitro* study of cell−scaffold interactions or *in vivo* tissue regeneration. These scaffolds aim to mimic the extracellular matrix, acting as a physical support and regulating the biological activity that affects cells such as migration, proliferation, and differentiation.[1] To achieve tissue repair, it is crucial to adapt scaffold stiffness to the targeted tissue, but also scaffold hydrophilicity and degradation rate. Macroporous polyesters, such as poly-ε-caprolactone (PCL) and poly(L-lactide) (PLLA), have been highly investigated in tissue engineering due to their excellent biocompatibility and inherent degradability through hydrolysis of their ester bonds. Nevertheless, the latter are essentially restricted to hydrophobic scaffolds and present limited tunability of their physicochemical properties and functionalities.

In contrast, polyphosphoesters (PPEs) comprising hydrolyzable phosphoester groups in their backbone are emerging synthetic biomaterials that combine biocompatibility, biodegradability, as well as molecular diversity.[2−4] Their physicochemical and biointerfacial properties can be easily tuned thanks to the pentavalent phosphorus atom present in their main chain, offering opportunities to design tailored macromolecular platforms for functional biomaterials. As recently demonstrated by comparing PPEs with phosphate or phosphonate moieties and bearing alkyl side chains of various lengths, the hydrolysis kinetics of PPEs can be tuned from minutes to years, depending on their microstructure.[4] *In vitro* studies showed that hydrophilic polyphosphate (Figure 1A) bearing an ethyl side chain readily undergoes hydrolytic degradation that can be further accelerated by enzymes.[5] Polyphosphate networks exhibit a wide range of mechanical properties with compressive moduli ranging from 20 kPa to over 700 MPa, opening prospects in both soft and hard tissue applications.[6,7] Tuning the length of the alkyl pendent groups[8] and the cross-linking degree[9] strongly impacted their hydrophilicity, degradation rate, and mechanical properties,[6,7] so that matching the cell interactions and tissue regeneration rate can be foreseen. The high versatility of the PPE structure has triggered intensive research activity for the design of PPE-based drug nanocarriers in the past decade,[10] and water-soluble

Received: December 11, 2024
Revised: February 7, 2025
Accepted: February 7, 2025
Published: February 17, 2025



Downloaded via UNIV CATHOLIQUE DE LOUVAIN on July 6, 2025 at 18:23:34 (UTC).
See https://pubs.acs.org/sharingguidelines for options on how to legitimately share published articles.

© 2025 American Chemical Society

https://doi.org/10.1021/acs.biomac.4c01740
Biomacromolecules 2025, 26, 1935−1947

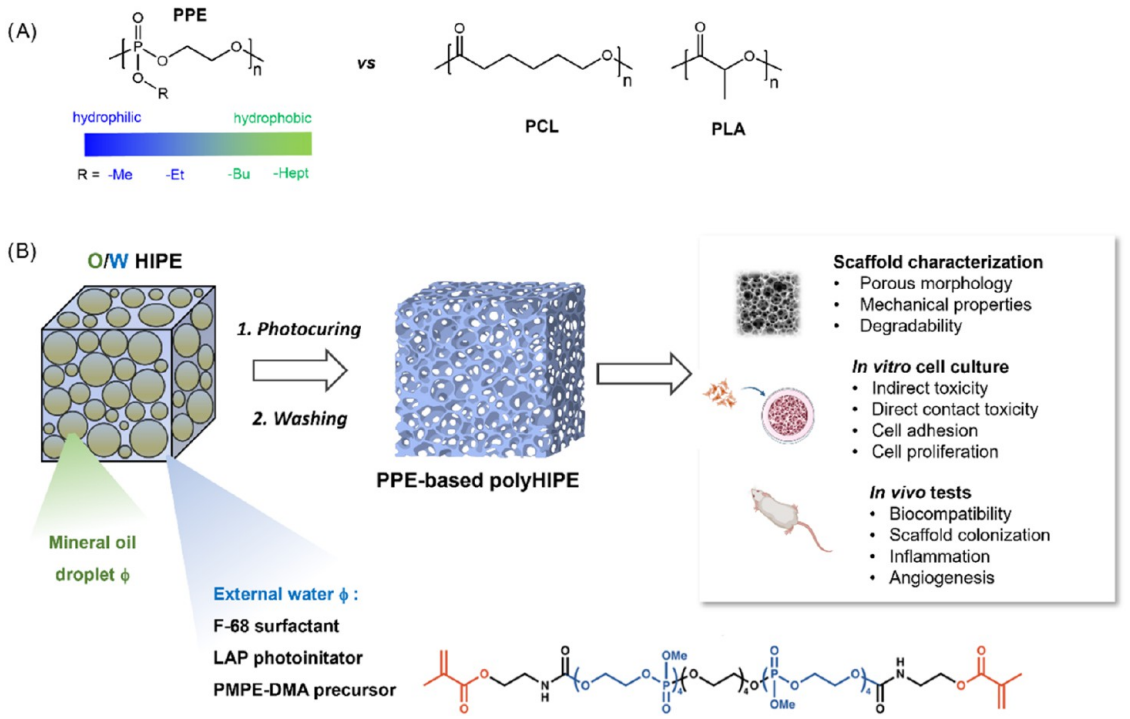


Figure 1. Structure of polyphosphoesters and polyesters (A) as well as a general strategy toward emulsion-templated PPE-based scaffolds (B).

PPEs are seen today as a degradable alternative to PEG for biomedical applications.[9] So far, a few pioneering works highlight the relevance of PPEs for tissue engineering. The surface modification of scaffolds with PLA−PPE showed enhanced osteoblast adhesion, proliferation, and function.[11] PPE hydrogels induced mineralization of bone marrow-derived mesenchymal stem cells (MSCs).[12] Remarkably, poly(ethyl sodium phosphate) PPEs represent intrinsically bioactive bone-scaffolds fastening osteoblastic cell proliferation, as demonstrated on a mouse model.[13] Fully degradable hyaluronic acid/PPE hydrogels were used for the growth of human MSCs.[14] A first example of 3D-structuration of poly(2-methacryloyloxyethyl phosphorylcholine) cross-linked with a PPE, namely, polyphosphate bearing methacrylic unsaturations, via a radical process, has been reported in the literature.[15] In this study, highly porous hydrogels were obtained by salt-leaching of potassium bicarbonate particles together with gas formation, but this process offered limited control over the pore size and low interconnectivity. It is a real limitation knowing the impact of pore size and interconnections on cell development and colonization of the scaffolds.[16]

An increasingly popular method for creating porous scaffolds for tissue engineering applications is high internal phase emulsion (HIPE)-templated polymerization[17,18] largely due to its simplicity, tunable porosity, scalability, and ease of shaping into various 3D constructs.[19,20] In practice, a polymer precursor located in the external continuous phase of an emulsion, where the volume of the internal phase exceeds 74%, is cured to fix the emulsion microstructure before removal of the sacrificial droplet phase.[21,22] The resulting polymerized HIPEs (polyHIPEs) exhibit a hierarchically structured and interconnected 3D morphology consisting of quasi-spherical "pores" connected by circular holes called "windows." Pore and window sizes can be tuned through the emulsification process, curing method, and nature and concentration of the surfactant, polymer precursors, and initiator.[17,18]

PolyHIPEs are effective scaffolds for tissue engineering and cell culture, with their open porous morphology enabling rapid mass transport of nutrients, gases, and waste, thereby supporting cell growth and proliferation.[23,24] Among others, polyester-based polyHIPEs have been widely used as scaffolds in tissue engineering, but their application is primarily limited to hydrophobic materials suitable for hard tissue regeneration such as bone healing.[24−29]

The present work aimed at structuring for the first time polyphosphoesters hydrogels into interconnected 3D-porous scaffolds and exploring their potential for tissue engineering, in particular, for soft tissue regeneration. A polymerizable hydrophilic PPE precursor was synthesized by ring-opening polymerization (ROP) and converted into interconnected macroporous PPE polyHIPEs via photocuring under oil-in-water (O/W) HIPE conditions (Figure 1B). The impact of the surfactant concentration and the volume ratio of the emulsion phases on the morphology (openness, pore, and interconnection sizes) and on the mechanical properties of the PPE-based polyHIPEs was evaluated. Scaffold degradability was investigated under physiological pH conditions. Indirect and direct contact toxicity toward human mesenchymal stem cells was also studied while cellular adhesion and cell proliferation were assessed. A PPE-based scaffold modified with the RGD peptide was also considered to further improve cellular adhesion. Finally, the scaffold biocompatibility was evaluated *in vivo* in a mouse subcutaneous implantation model. This study as a whole confirms that PPE porous materials hold great promise for tissue engineering.

2. MATERIALS AND METHODS

2.1. Materials. 2-Chloro-2-oxo-1,3,2-dioxaphospholane (COP, 95%, TCI), tetraethylene glycol (99%, Sigma-Aldrich), 2-isocyanatoethyl methacrylate (98%, stabilized with BHT, TCI), dry tetrahydrofuran (THF, VWR), dry dichloromethane (DCM, VWR), hydroquinone (99%, Sigma-Aldrich), Pluronic F-68 (Sigma-Aldrich),

https://doi.org/10.1021/acs.biomac.4c01740
Biomacromolecules 2025, 26, 1935−1947

lithium phenyl-2,4,6-trimethylbenzoylphosphinate (LAP, 95%, Sigma-Aldrich), 3-D Life RGD peptide (Cellendes, RGD-SH, RGD motif with thiol group on the N-terminus), mineral oil (Sigma-Aldrich), and ethanol (99%, Technisolv) were used as received. Methanol (MeOH, VWR Chemicals), triethylamine (TEA, 99.5%, Sigma-Aldrich), and 1,8-diazabicyclo[5.4.0]undec-7-ene (DBU, 98%, Sigma-Aldrich) were dried over calcium hydride (93%, Thermo Scientific) and distilled under reduced pressure before being used. N-cyclohexyl-*N*′-(3,5-bis(trifluoromethyl)phenyl)thiourea (TU) was synthesized in the lab according to established protocol.[30]

2.2. Synthesis of 2-Methoxy-2-oxo-1,3,2-dioxaphospholane (MEP). Dry THF (175 mL), dry MeOH (7.6 mL, 175 mmol), and dry TEA (25 mL, 180 mmol) were introduced into a 500 mL flame-dried two-necked flask equipped with a 100 mL addition funnel charged with a solution of COP (25 g, 175 mmol) and dry THF (25 mL). The solution was added dropwise in the flask while stirring at 0 °C under an argon atmosphere and left overnight. The triethylammonium salt formed during the reaction is removed through filtration, and the THF was evaporated. The concentrated residue was purified by fractional distillation at low pressure between 80 and 90 °C, leading to a colorless liquid MEP (14.84 g, 107 mmol, yield: 61%). The monomer was dissolved in $CDCl_3$ and characterized by ^1H and ^{31}P NMR (Bruker 400 MHz, 25 °C, TMS internal reference). The recorded spectra were analyzed via MestReNova software (14.1.0). The chemical shifts for the ^1H spectrum are referenced relative to $CDCl_3$ at 7.26 ppm. ^1H NMR: δ = 4.61−4.31 (m, 4H), 3.87 (d, 3H) ppm. ^{31}P NMR: δ = 18.64 ppm.

2.3. Synthesis of Dimethacrylated Poly(2-methoxy-2-oxo-1,3,2-dioxaphospholane) (PMEP-DMA). Tetraethylene glycol (0.53 g, 2.7 mmol) and TU (1.33 g, 3.6 mmol) were introduced into a 100 mL flame-conditioned flask and dried using three cycles of azeotropic distillation with toluene. MEP (3 g, 21.6 mmol) was added into the flask and placed under vacuum for 15 min. Dry dichloromethane (10 mL) was then introduced under an argon atmosphere. The polymerization was initiated by adding dry DBU (1.8 mL, 12 mmol) at 0 °C and stirring for 45 min. The reaction was terminated by adding an excess of 2-isocyanatoethyl methacrylate (1.5 mL, 10.6 mmol) and was stirred for 30 min at 25 °C. The polymer was precipitated twice in ice-cold diethyl ether. The viscous polymer was collected with MeOH, and 0.7 mol % of hydroquinone was added before being dried under vacuum for 24 h. ^1H NMR (400 MHz, $CDCl_3$, 25 °C): δ = 6.11 (s, 2H), 5.57 (s, 2H), 4.34−4.14 (m,44H), 3.83−3.73 (m, 24H), 3.72−3.66 (m, 4H), 3.65−3.59 (m, 8H), 1.93 (s, 6H) ppm. ^{31}P NMR: δ = 1.11, −0.16, −1.46 ppm.

2.4. Preparation of PolyHIPE Scaffolds. PPE polyHIPEs were produced through photopolymerization according to the formulation presented in Table S1 in 4 mL flasks with a diameter of 14.7 mm. First, the PMEP-DMA, the surfactant (Pluronic F-68), and the photoinitiator (LAP) were dissolved in Milli-Q water in the flask. The mineral oil was then added dropwise to the aqueous solution under vortex agitation in order to create the high internal phase emulsion. The HIPE was then placed under an argon atmosphere before curing by UV irradiation for 15 min (TENMA DC power supply, I < 0.5 A, λ = 365 nm). After unmolding, the samples were washed successively for 24 h in DCM, 24 h in MeOH, and 24 h in distilled water. Samples dedicated to the *in vitro* and *in vivo* experiments were immersed in a 70% ethanol solution for 48 h and washed 3 times with sterile PBS before use. Inspired by a previously reported efficient RGD grafting procedure,[31] the same emulsion polymerization protocol was carried out in the presence of RGD-SH (0.68 mol % of RGD-SH compared to the methacrylate groups was solubilized in the aqueous phase) for the preparation of the RGD-modified PPE scaffolds dedicated to cell culture and in vivo tests.

2.5. Morphological Characterization of PolyHIPE Scaffolds. The morphology of the polyHIPE was characterized with SEM. First, a rectangle was cut in the middle of the sample to access the internal cross section. The rectangles were freeze-dried in a glass vial coated with a PTFE film before being mounted on aluminum stubs with double-sided carbon tape. Then, the polyHIPEs were sputter-coated with gold for 60 s (Balzers SCD 004 sputter coater (BAL-TEC)) before being imaged using a Quanta 600 SEM operating at 20.0 kV. The images were analyzed using ImageJ 1.53, where the diameters of 150 pores and 200 windows were measured from three different polyHIPEs for each formulation. A statistical correction was applied to the average pore size.[5,17] The degree of openness (DOO) was calculated on 9 pores for each formulation by dividing the open surface by the surface of the pores.[18]

2.6. Mechanical Characterization of PolyHIPE Scaffolds. The mechanical properties of the polyHIPE scaffolds are measured with a dynamical mechanical analysis (DMA) Q800 instrument (TA Instruments) equipped with a compression module. Three polyHIPEs were tested for each formulation, and the Young's modulus was calculated in the linear-elastic region of every curve.

The samples consist of 10 mm height and 15 mm diameter cylinders. The stress−strain curves were recorded at room temperature with a compression speed of 100 μm/mm.

2.7. Degradability Assessment of PolyHIPE Scaffolds. The hydrolytic degradation of the PPE polyHIPE scaffolds was assessed through three different methods after the samples were left at 37 °C under soft shaking for different predetermined time intervals. The first method was the measurement of the swelling in bicarbonate/carbonate (HCO_3^-/CO_3^{2-}) buffer (pH = 10.6) by measuring the diameter of the monolith. The second test consists of assessing the evolution of the supernatant pH. A PPE polyHIPE was placed in a vial with ultrapure water, and the pH was measured after several time periods (HI 2211 pH/ORP meter, HANNA instruments). And finally, the mechanical properties over time in PBS were also measured following the already described protocol to assess the Young's modulus.

2.8. Impact of PPE Scaffolds on SCAP *In Vitro*. *2.8.1. Stem Cell of the Apical Papilla (SCAP Luc+) Culture.* Human SCAP (RP89)[32] cells were transduced with the lentiviral vector TM914 containing the firefly luciferase gene in Prof. Michiels' lab (de Duve Inst., Univ. of Louvain), as described by Lizcano-Perret et al.[33] SCAP Luc+ express the firefly luciferase gene under the control of the phosphoglycerate kinase gene promoter.[34] They were used to assess cell viability when in direct or indirect contact with polyHIPE scaffolds.

SCAP were cultured in an incubator at 37 °C and 5% CO_2 in Dulbecco's modified Eagle medium (DMEM, Sigma-Aldrich), 10% fetal bovine serum (FBS, Sigma-Aldrich), and 1% penicillin/streptomycin (Pen/Strep, Thermo Fischer Scientific) in T75 and T175 flasks. The medium was changed every 2−3 days until confluence. Cells were used between the third and seventh passages.

2.8.2. Cytotoxicity. For both direct and indirect cytotoxicity tests, 15,000 cells were seeded in a 96- nontreated well plate at a density of 1,500,000 cells/ml. Then, 200 μL of sterile medium was added to the well, and the cells were incubated at 37 °C at 5% CO_2 for 4 h. For the indirect toxicity test, the medium was then replaced with 200 μL of sterile medium previously conditioned by incubation with a polyHIPE scaffold for 48 h. For direct toxicity, the medium was replaced by 200 μL of sterile medium, and a piece of polyHIPE scaffold was placed in direct contact with the cells at the bottom of the well. For both cytotoxicity tests, SCAP were then further incubated at 37 °C at 5% CO_2 for 24 h. The medium and the polyHIPE were then removed, and 200 μL of a 10 vol % PrestoBlue (InVitrogen, Thermo Fischer Scientific) solution was added and incubated for 2 h at 37 °C. Then, 10 μL of the reacted PrestoBlue solution was transferred from each well in a 96 black well plate and measured on a spectrofluorometer (SpectraMax iD5, Molecular Devices, San Jose, CA) at an excited wavelength of 560 nm and an emission wavelength of 590 nm.

2.8.3. Cell Viability. Scaffolds were placed in a 24-cell-repellent well plate, and 100,000 cells were seeded on top at a concentration of 5,000,000 cells/mL. After 1 h of incubation at 37 °C, 500 mL of medium was carefully added to each well. The medium was changed every 2−3 days. After 1, 4, and 7 days, the medium was removed, and the scaffolds were collected and placed at −80 °C until further analysis. Samples were then thawed on ice before adding 200 μL of One-Glo Luciferase Assay solution (Promega) per tube and processing the samples as per the supplier's instructions. Results

https://doi.org/10.1021/acs.biomac.4c01740
Biomacromolecules 2025, 26, 1935−1947

Table 1. Emulsion-Templated PPE-Based Scaffolds

entry	samples	surfactant (wt %)[a]	O/W (v/v)[b]	D (μm)[c]	d (μm)[d]	DOO[e]	E (kPa)[f]
1	PH_1	10	85/15	16.3 ± 7.0	2.4 ± 0.8	0.19	10.6 ± 1.1
2	PH_2	5	85/15	16.7 ± 5.9	3.1 ± 1.2	0.29	9.3 ± 3.4
3	PH_3	1.25	85/15	18.1 ± 4.9	3.6 ± 1.0	0.32	11.3 ± 3.1
4	PH_4	1.25	75/25	20.4 ± 3.8	3.6 ± 1.0	0.16	42.3 ± 0.4
5	PH_5	1.25	80/20	18.8 ± 4.5	3.4 ± 1.0	0.26	33.6 ± 3.3
6	PH_6	1.25	90/10	18.1 ± 4.9	3.8 ± 1.1	0.36	3.3 ± 0.4

[a]Conditions: external phase = mineral oil, PMEP-DMA (50 wt % compared to aqueous phase), LAP (1.33 wt % compared to the aqueous phase), photocuring (15 min, λ = 365 nm). Surfactant = F-68 (wt% compared to the aqueous phase). [b]volume ratios between the internal oil phase and the external aqueous phase. [c]Mean pore diameter. [d]Mean window diameter. [e]Degree of openness. [f]Young's Modulus measured by compression tests.

were analyzed by using a standard calibration curve representing the bioluminescence as a function of the number of cells.

2.8.4. Cell Morphology. The scaffolds were seeded with SCAP, as described in 2.8.3. After 1, 4, and 7 days of culture, the scaffolds were transferred to a 24-well plate, washed twice with PBS, and then fixed with 1 mL of 4 vol % formaldehyde (PFA, Carl Roth GmbH). Samples were washed twice with PBS and incubated for 20 min in 400 μL of immunocytochemistry (ICC) buffer (1 vol % BSA and 0.1 vol % Triton-X100 in PBS) at RT. Then, samples were incubated for 1 h with 400 μL of DAPI/phalloidin staining solution (1:1000 DAPI (Sigma-Aldrich) and 1:1000 rhodamine phalloidin (Thermo Fischer Scientific) in PBS). The scaffolds were then stored at 4 °C in PBS before imaging on a high-resolution confocal microscope (Zeiss LSM 980 Airyscan 2).

2.9. PolyHIPE Scaffold Biocompatibility. *2.9.1. Subcutaneous Implantation Mouse Model.* All of the experiment protocols were approved by the Ethical Committee for Animal Care of the Université Catholique de Louvain Medicine Faculty (2023/UCL/MD/73). The PPE scaffolds (with and without RGD) were trimmed to create cylinders with a diameter of 8 mm and a thickness of 2 mm. They were then sterilized by soaking in 70 vol % ethanol for 24 h before being washed 3 times with sterile physiological serum. Swiss female mice (6−8 weeks old) were shaved with an electric razor on both flanks, treated with Veet gel hair removal cream, and disinfected. Prior to the surgery, mice were subcutaneously injected with buprenorphine (0.1 mg/kg) and then sedated with isoflurane (2% in oxygen). Once anesthetized, a 10 mm incision was made on the flank to insert the scaffold, and then skin was sutured using surgical staples. The operation was repeated on the other flank. The health and weight of the mice were closely monitored during the time of the experiment.

2.9.2. Immunohistological Analysis of Angiogenesis and Immune Cell Infiltration. After 1 and 4 weeks, the mice were deeply sedated with isoflurane and then euthanized by dislocation. The scaffolds were retrieved and placed in a tissue cassette. The cassette was then immersed in a 4% formaldehyde solution for 24 h before being washed 3 times with PBS. Finally, the scaffolds were cut in half to reveal the inner section of the cylinder, embedded in paraffin (Tissue-TEK VIP, Sakura Europe, Japan), and stored at room temperature until further analysis.

A series of 5 μm thick sections of the scaffolds were produced with a microtome and stained with hematoxylin-eosin (H&E) and Masson's trichrome. Concerning immunohistochemistry (IHC), heat-induced antigen retrieval was performed with citrate buffer (pH 5.7). Endothelial cells were stained using anti-CD31/PECAM1 (1:100 dilution, 77699S, Cell Signaling Technology) and immune cell infiltration using anti-CD45 (1:100 dilution, D3F8Q, Cell Signaling Technology) primary antibodies. Samples were incubated overnight at room temperature with primary antibodies and with a secondary antirabbit-HRP antibody (EnVision+ Single Reagent, K4003, DAKO) for 1 h. After development with DAB substrate (3,3′-Diaminobenzidine, K3468, DAKO), slides were counterstained with hematoxylin (S3301, DAKO) and mounted with coverslips. All of the images were captured using a digital slide scanner (Pannoramic ScanII, 3DHistech, Hungary) and analyzed with software ImageJ 1.53 and QuPath.

2.10. Statistical Analysis. All statistical analyses were made with one-way or two-way ANOVA using GraphPad Prism 10.1.1 software. A p-value <0.05 was considered statistically significant. All displayed value are the average ± standard deviation.

3. RESULTS AND DISCUSSION

3.1. Fabrication of Polyphosphoester PolyHIPE Scaffolds. As a precursor of the emulsion-templated hydrophilic PPE scaffolds, we considered a hydrosoluble dimethacrylated PPE derivative with methoxy pendant groups (PMEP-DMA). Inspired by a procedure reported by Wurm et al.,[35] this precursor was synthesized by sequential ROP of 2-methoxy-2-oxo-1,3,2-dioxaphospholane (MEP) and conversion of the terminal hydroxy function by reaction with 2-isocyanatoethyl methacrylate (Figure S1). Note that the resulting urethane linker moieties are likely to contribute to the enhancement of the mechanical properties of the porous hydrogels through the formation of hydrogen bonds. The MEP polymerization was carried out at 0 °C in dichloromethane using tetraethylene glycol (TEG) as a difunctional initiator ([MEP]/[TEG] = 8) in the presence of DBU and TU as metal-free catalyst/cocatalyst (stoichiometric amount compared to alcohol functions), followed by addition of a 2-fold excess of isocyanate functionalizing agent. Besides typical signals of the MEP repeating units, ^{1}H NMR analysis of the PMEP-DMA exhibited peaks characteristic of the olefinic hydrogens of the terminal methacrylate groups (Figure S2A). The degree of polymerization and functionalization rate were estimated at 8 (corresponding to an $M_{n\ NMR}$ of 1600 g/mol) and 94%, respectively. The ^{31}P NMR spectrum showing typical phosphorus signals at −0.16 ppm for the main repeating units and 1.07 and −1.49 ppm for the terminal units further confirmed the structure of the PMEP precursor (Figure S2B).

The PPE scaffolds were then produced via high internal phase emulsion (HIPE) templating radical photopolymerization of PMEP-DMA. PMEP-DMA was photocured in the continuous external aqueous phase of an oil-in-water (O/W) HIPE using mineral oil as the droplet phase. According to the Bancroft rule,[36] we selected a surfactant widely used in biomedical applications with a high HLB (HLB = 29), namely, the Pluronic F-68, that will be more soluble in the aqueous phase and thus favorable to the stabilization of O/W HIPEs. After emulsification by dropwise addition of the oil phase under vortex stirring, PMEP-DMA was cured by irradiation at 365 nm for 15 min using LAP as the photoinitiator. The latter was preferred over Irgacure 2959 due to its lower cytotoxicity and increased water solubility.[37] This emulsion templating polymerization was performed with different concentrations of surfactant and various O/W phase volume ratios in the HIPE regime to possibly modulate the morphology and mechanical properties of the porous materials. The results are summarized in Table 1.

https://doi.org/10.1021/acs.biomac.4c01740
Biomacromolecules 2025, 26, 1935−1947

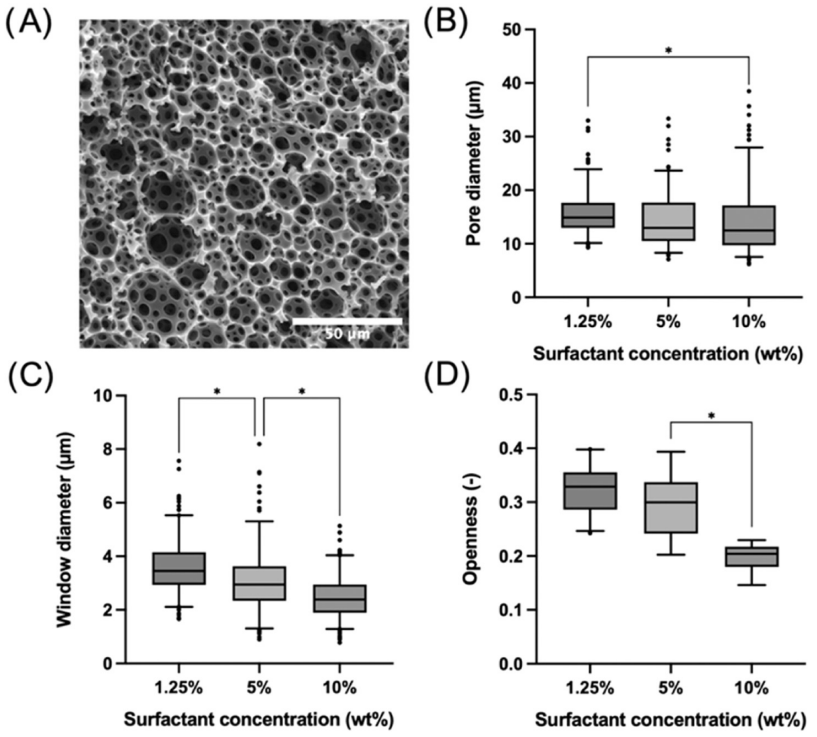


Figure 2. Scanning electron microscopy image of polyHIPE PH_3 (A) as well as box-and-whisker plots of pore diameter (B), window diameter (C), and DOO (D) of PPE polyHIPEs as a function of the surfactant concentration. (* = p-value <0.05).

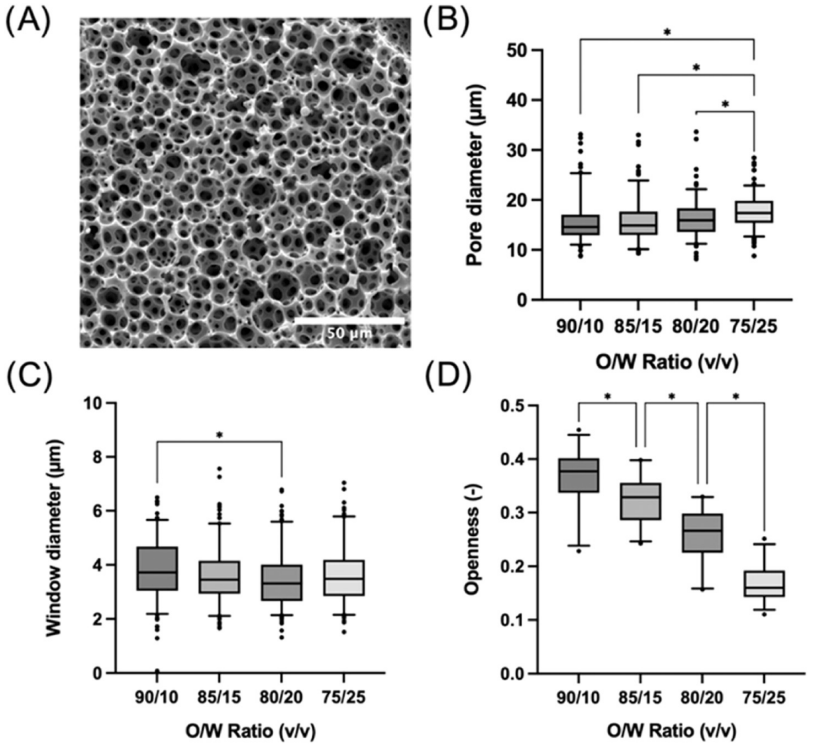


Figure 3. Scanning electron microscopy image of polyHIPE PH_6 (A) as well as box-and-whisker plots of pore diameter (B), window diameter (C), and DOO (D) of PPE polyHIPEs as a function of the O/W v/v ratio. (* = p-value <0.05).

A first series of HIPE polymerizations was conducted with 10, 5, 1.25, and 0.625 wt % of F-68 in the aqueous phase, keeping the O/W volume ratio constant at 85/15. Except for the lowest concentration of stabilizer for which rapid demixing of the emulsion was observed, stable HIPEs were formulated and successfully converted by photocuring into the corresponding polyHIPEs PH_{1-3} (Table 1, entries 1−3). After washing and lyophilization of monoliths, SEM analysis evidenced that PH_{1-3} featured the characteristic porous structure of polyHIPEs with pores interconnected by windows

https://doi.org/10.1021/acs.biomac.4c01740
Biomacromolecules 2025, 26, 1935−1947

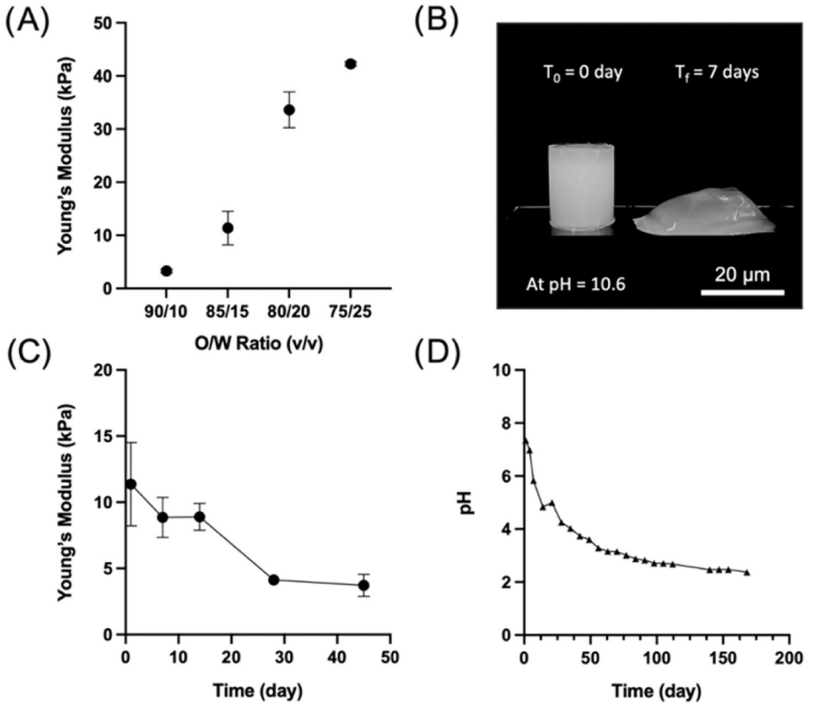


Figure 4. Young's modulus of PPE polyHIPEs as a function of the O/W (v/v) ratio (A). Images of the PH_3 scaffold before (left) and after (right) being immersed for 7 days in a basic buffer (pH = 10.6) (B). Evolution of the Young's modulus of the scaffold PH_3 after being immersed in PBS (pH = 7.4) for different time periods (C). Evolution of the PPE scaffold supernatant pH over time (D).

(Figures 2A and S3). A closer examination of the SEM images also indicates that the size of the pores (average diameter from 16 to 18 μm) and windows (average diameter from 2.4 to 3.6 μm) do not vary markedly with the concentration of the surfactant (Figure 2B,C, respectively). Only a slight increase of pore and window dimensions is observed when decreasing the amount of F-68. A more significant trend is observed between the degree of openness (DOO) and the surfactant concentration (Figure 2D), with the highest interconnectivity (DOO = 0.32) being measured for PH_3 formulated with the lowest amount of surfactant. This observation appears to contradict recent theories on the mechanism of pore formation, suggesting that pores result from the removal of surfactant-rich domains between the neighboring droplets during the post-curing treatment.[38] According to this principle, reducing the surfactant concentration should limit interconnections. In our study, the macromolecular nature of the surfactant and the use of water as a porogenic solvent in the external phase may explain the deviation from this trend, confirming that the formation of interconnected pore structures is a complex phenomenon and still requires investigation. Nonetheless, 1.25 wt % of F-68 was sufficient to provide a highly interconnected PPE-based polyHIPE structure. Using such a low concentration of surfactant in the formulation also reduces the risk of incomplete removal of the latter from the materials, thereby minimizing its impact on the scaffolds' properties.

Next, the HIPE templating polymerization of PMEP-DMA was carried out with different O/W volume ratios, namely, 90/10, 80/20, and 75/25, using F-68 at 1.25 wt % in the aqueous phase to favor the openness of the material (Table 1, entries 4−6). Proper stabilization of the HIPE occurred in all cases, leading to PH_{4-6} after irradiation. As illustrated by SEM images in Figures S3 and 3A, the three formulations led to polyHIPEs with similar average pore size (18−20 μm) and window size (3.4−3.6 μm) (Figure 3B,C). In contrast, increasing the volume percentage of the internal phase from 75 to 90% increased the degree of openness of the polyHIPEs from 0.16 (for PH_4) to 0.36 (for PH_6) (Figure 3D). The greater openness of PH_6 is rationalized by the higher deformation of the droplets occurring at a high concentration of dispersed phase, favoring the formation of the interconnects. Overall, the PPE-based scaffolds feature interconnected porous morphologies suitable for the colonization of the scaffold by cells.

3.2. Mechanical Properties and Degradation. One crucial feature of polymer scaffolds dedicated to TE is their ability to mimic the natural extracellular matrix (ECM) of the targeted tissues in terms of mechanical properties.[39] Controlling the stiffness of scaffolds is also key, as interactions of cells with the support activate the mechano-transduction pathways by which cells convert mechanical stimuli from their surroundings into biochemical signals, which regulates various cellular functions.[39] Therefore, the PPE-based polyHIPEs (PH_{1-6}) were subjected to compression tests via dynamical mechanical analysis (DMA) in their hydrated state to measure their mechanical properties, particularly the Young's modulus (Figures 4A and S4, Table 1).

Because their formulation only differs by the amount of surfactant and their porous structures are comparable, PH_{1-3} exhibit similar Young's modulus (Figure S4). In these cases, an O/W volume ratio of 85/15 was used, leading to a rather low Young's moduli around 10 kPa. In contrast, a significant trend was observed for the Young's modulus of PH_{3-6} formulated with various O/W volume ratios, and so with different amounts of PPE precursor in the final scaffold (Figure 4A). Indeed, the Young's modulus increased from 3.3 kPa for PH_6 to 42.3 kPa for PH_4 when the O/W volume ratio changed from 90/10 to 75/25. In the latter case, a higher proportion of

https://doi.org/10.1021/acs.biomac.4c01740
Biomacromolecules 2025, 26, 1935−1947

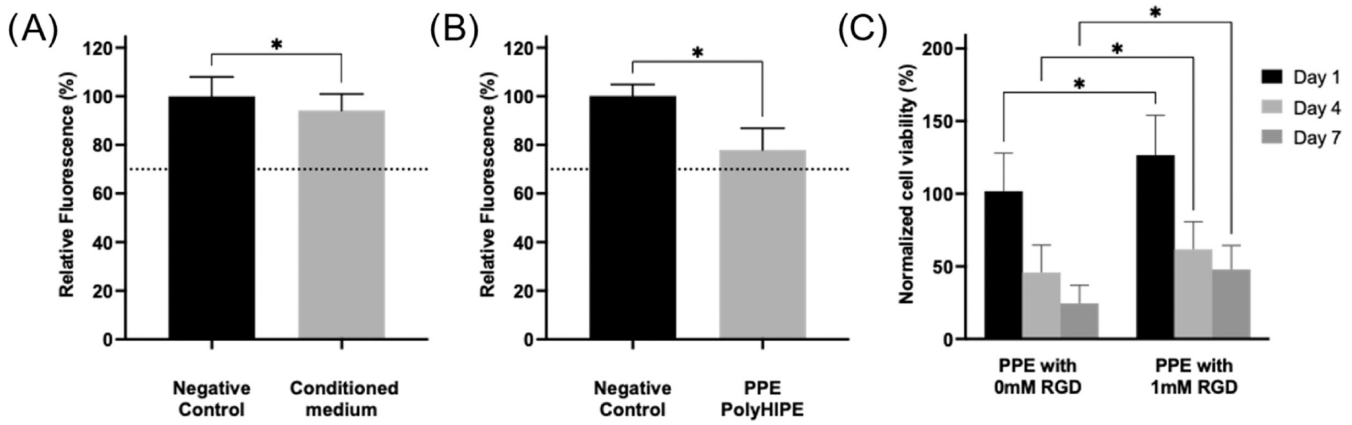


Figure 5. Indirect toxicity of the PPE polyHIPE (A), direct contact toxicity of the PPE polyHIPE (B), and bioluminescence assessment of the unmodified and RGD-modified PPE scaffold PH_3 after 1, 4, and 7 days of culture (C).

aqueous phase containing 50 wt % of PPE-DMA was used, leading to stiffer scaffolds. Overall, the emulsion-templated PPE-based scaffolds present tunable and low Young's modulus that could be appropriate for soft tissues such as the brain (0.1−1 kPa), pancreas (1−5 kPa), skin, and muscle (5 kPa to 140 MPa).[39−42]

Degradability is another important characteristic of the scaffolds, which ensures a seamless transition from the scaffold to natural tissues while minimizing problems associated with long-term implantation. Although the degradability of PPEs is well documented,[2,5,8,9,35] the degradation rate of these emulsion-templated PPE-based scaffolds was evaluated in order to highlight a potential effect of the porous structure on the rate of the degradability of the matrix. For this study, we selected PH_3, which presented a good compromise in terms of openness and mechanical properties. As a preliminary test, scaffold PH_3 was immersed in basic buffer (pH = 10.6), since rapid degradation of PPE is reported under basic conditions (Figure 4B).[4,8,43] After 7 days in the basic buffer, PH_3 completely lost its mechanical properties, confirming the hydrolytic degradation of the PPE. The collapse of the scaffold reflects a bulk degradation rather than a surface erosion occurring due to the open porous structure. The degradability of polyHIPE was then investigated in more detail at physiological pH in PBS by monitoring its mechanical properties over time via compression tests (Figure 4C). As expected, the Young's modulus dropped from 11 to 4 kPa over 45 days as a result of the degradation of the PPE matrix. After 60 days, the degradation process was so advanced that Young's modulus could no longer be measured. The degradation of the PPE scaffold was monitored in ultrapure water by following the pH change of the supernatant resulting from the release of phosphoric acid-based degradation products. As shown in Figure 4D, the pH of the solution decreased steadily toward 2.14 corresponding to the pK_a of phosphoric acid, confirming their degradability through phosphoester bond hydrolysis. In summary, significant degradation of the PPE polyHIPE in PBS occurred over approximately 4 to 8 weeks, which aligns with Wurm's observations on the corresponding nonporous PPE hydrogels.[35] This ensures that the porosity of the PPE-based polyHIPEs does not drastically accelerate the degradation of the material, which can provide cell support during the regeneration period.

Overall, the PPE-based scaffolds feature valuable morphological, mechanical, and physicochemical properties for tissue engineering applications and warrant a close examination of their biological performance *in vitro* and *in vivo*.

3.3. Impact of the Scaffolds on Cell Viability and Adhesion. The cytocompatibility of the scaffolds was initially assessed through both indirect and direct contact cytotoxicity tests using the PrestoBlue assay kit. If the absence of cytotoxicity was already reported for PPEs films,[9,11] it has to be confirmed for the porous polyHIPE scaffolds. For the indirect cytotoxicity tests, the PPE scaffolds were placed in sterile culture medium for 48 h to allow the possible release of any residues from the scaffold synthesis or degradation products. The polyHIPE scaffolds were then removed, and the resulting conditioned medium was added to stem cells of the apical papilla transduced to express firefly luciferase (SCAP Luc+). After 24 h of culture in the conditioned medium, cell viability only decreased by a few percent compared to the negative control (nontreated cells) but remained well above 70% (limit set according to ISO EN 10993-5 protocol criteria) (Figure 5A). This emphasizes the absence of indirect toxicity due to leaching. In the direct contact assay, the PPE scaffolds were placed in contact with SCAP to evaluate their intrinsic cytotoxicity. The cell viability decreased to 77% after 24 h (Figure 5B). This value is a bit lower compared to the one recorded in the indirect cytotoxicity test, possibly due to a slightly lower access to nutrients for the cells in direct contact with the scaffold. However, it is still higher than the critical value of 70%, confirming the limited toxicity of the PPE porous scaffolds even in close contact with cells in line with the cytocompatibility of previously reported PPE-based linear polymers or nonporous hydrogels.[9]

Next, the impact of the PPE scaffold surface on SCAP adhesion was studied. For this purpose, scaffolds were seeded with SCAP Luc+. The bioluminescence provides a quantitative measure of the number of viable cells on the scaffold after 1, 4, and 7 days (Figure 5C). After 1 day, cell viability was 101 ± 26%, but it then decreased to 45 ± 18 and 24 ± 12% after 4 and 7 days, respectively. We hypothesized, based on the evidenced lack of cytotoxicity of the PPE scaffolds, that this decrease in cell viability might be due to a low cell adhesion on the porous PPE scaffold, resulting on the removal of the nonadherent cells during culture medium changes. This assumption is consistent with the very low cell adherence recorded previously for nonporous PMEP hydrogels,[35] in line with the low protein adhesion properties of hydrophilic PPE sequences.[44] To validate this hypothesis and to increase cell

https://doi.org/10.1021/acs.biomac.4c01740
Biomacromolecules 2025, 26, 1935−1947

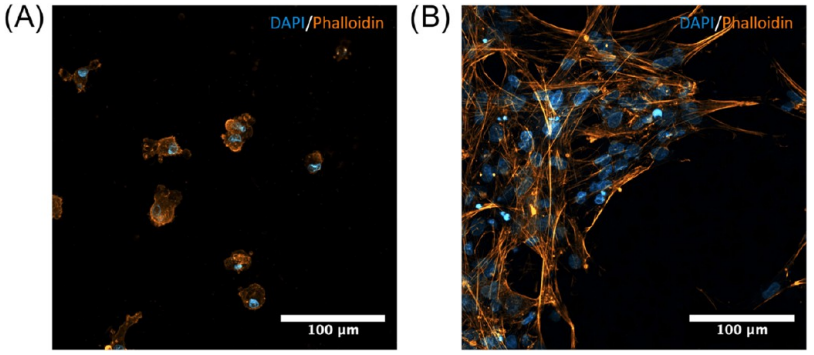


Figure 6. CLSM images of cell morphology after 1 day of culture on the unmodified (A) and the RGD-modified (B) PPE scaffold PH_3 (DAPI: nuclei are in blue; rhodamine phalloidin: actin filament in orange).

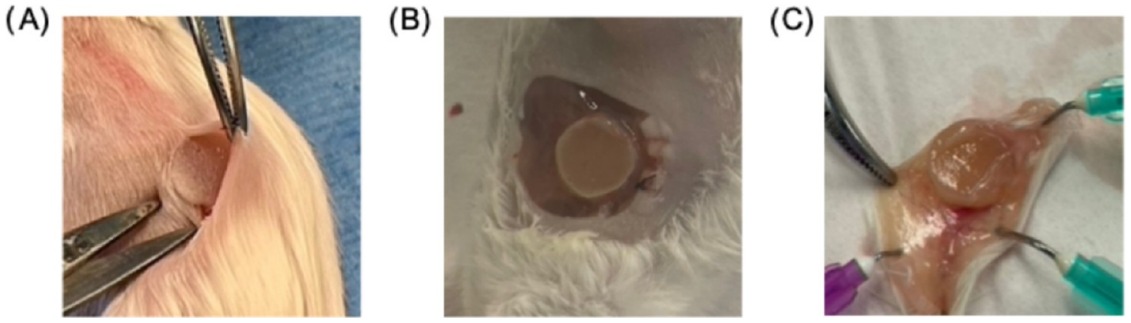


Figure 7. Subcutaneous implantation of the PPE scaffold in female Swiss mice through a 10 mm skin incision (A). PPE scaffolds at the implantation site during their retrieval after 1 week (B) and 4 weeks (C).

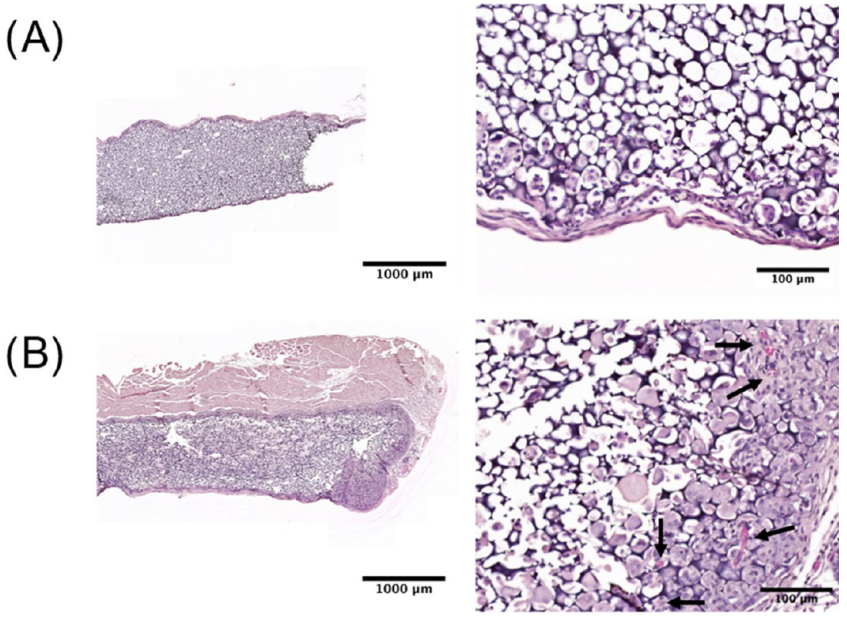


Figure 8. Cross sections and corresponding highlighted region of RGD-modified PPE-based scaffolds (A and B) stained with H&E after subcutaneous implantation in mice for 1 week (A) and 4 weeks (B).

adhesion, the PPE polyHIPE scaffold surface was modified for the first time with an RGD-based cell adhesion promotor.[45] In practice, RGD-functionalized PPE-based scaffolds were produced by emulsion templating polymerization carried out in the presence of a thiol-functionalized RGD peptide. The latter reacts *in situ* through thiol−ene click chemistry with terminal methacrylate functions of the PPE precursor in parallel to the photo-cross-linking reaction. RGD functionalization of the scaffold globally improved the cell adhesion (Figures 6A,B and S5) and, consequently, cell viability, even if it still decreased with time, from 126% after 1 day to 48% after 1 week (Figure 5C). These *in vitro* studies emphasize for the first time the benefit of grafting RGD to the surface of a PPE-based matrix for cell adhesion and culture.

3.4. *In Vivo* Biocompatibility of PolyHIPE Scaffolds. The objective was here to perform a biocompatibility study to

https://doi.org/10.1021/acs.biomac.4c01740
Biomacromolecules 2025, 26, 1935−1947

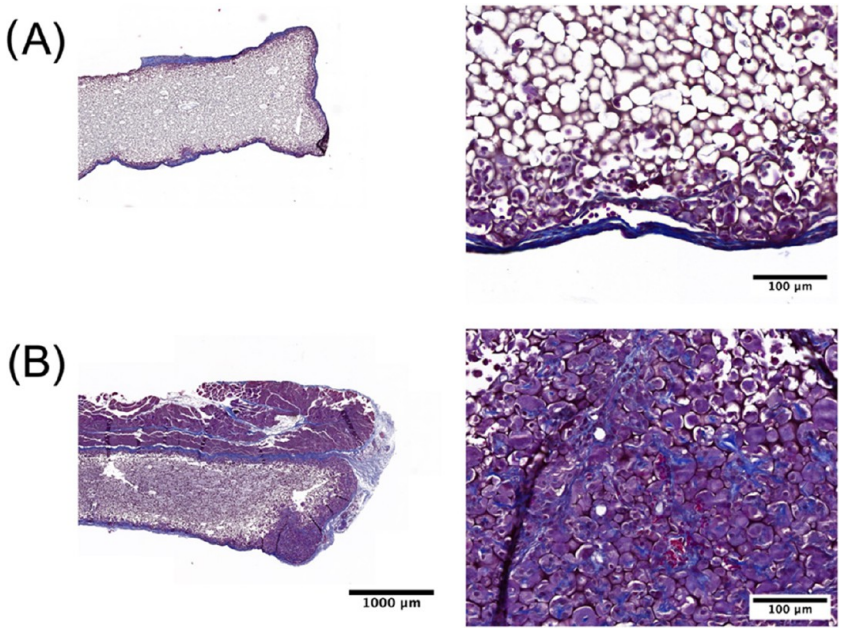


Figure 9. Cross section and corresponding highlighted region of RGD-modified PPE-based scaffolds stained with Masson's trichrome after subcutaneous implantation in mice after 1 week (A) and 4 weeks (B).

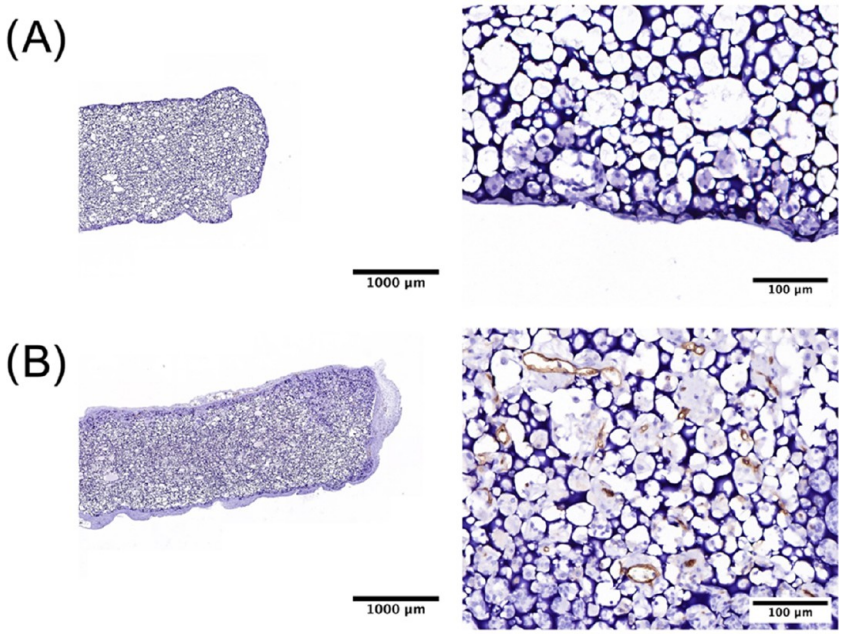


Figure 10. Cross section and corresponding highlighted region of RGD-modified PPE-based scaffolds stained with anti-CD31 (brown) to identify endothelial cells to confirm angiogenesis after 1 week (A) and 4 weeks (B).

assess the relevance of PPE polyHIPE scaffolds for TE applications. The biocompatibility of the scaffolds was evaluated by using a mouse subcutaneous implantation model. To the best of our knowledge, the *in vivo* implantation of a material primarily composed of polyphosphoester has not been investigated previously.

RGD-grafted PPE polyHIPE scaffolds were implanted for 1 and 4 weeks (with nongrafted ones as controls). Two scaffolds were implanted per mouse after aseparate skin incision on their flanks (Figure 7A). Mice did not exhibit visible inflammation, infection, or necrosis resulting from prolonged contact with the foreign scaffold. Healthy tissues and angiogenesis were observed surrounding the implanted scaffolds at all resection time points (Figure 7B,C). After 4 weeks, the skin and peritoneum adhered to the scaffold, reflected by a more difficult scaffold retrieval compared to 1 week.

Cell infiltration and proliferation were first evaluated by staining with H&E of the RGD-PPE polyHIPE scaffolds implanted for 1 and 4 weeks. After 1 week, infiltrating cells penetrated the scaffold but remained located at its periphery (Figure 8A). After 4 weeks, however, a significant increase in the cellular population was observed, with further cell infiltration within the scaffold porosity. In Figure 8A,B, the porous scaffold appears stained dark blue.

https://doi.org/10.1021/acs.biomac.4c01740
Biomacromolecules 2025, 26, 1935−1947

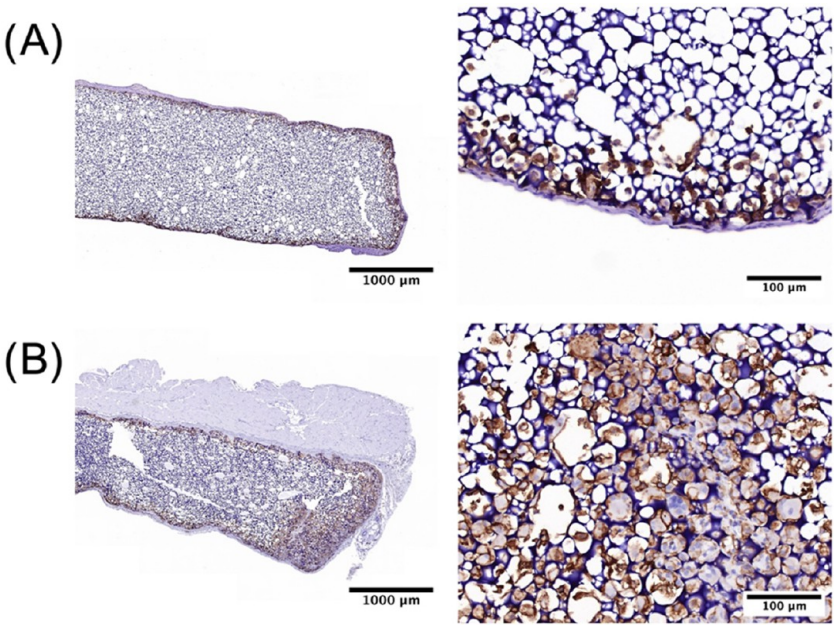


Figure 11. Cross section and corresponding highlighted region of RGD-modified PPE-based scaffolds stained with anti-CD45 (brown) to identify the immune response after 1 week (A) and 4 weeks (B).

Capsulation around the implanted scaffolds is observed and consists of the peritoneum, which is a common response to scaffold implantation and integration. The comparison of the scaffold after 1 and 4 weeks clearly demonstrated progressive degradation over time. Parts of the pore walls degraded, resulting in a less defined and less compact porous structure after 4 weeks, leaving a place for cell proliferation (Figure 8B). As a promising indication of the tissue restoration process, some red blood cells were observed inside newly formed vascular structures (see black arrows in Figure 8B). Similar observations were made for the unmodified PPE scaffolds (Figure S6). In contrast to the *in vitro* experiments, functionalizing the scaffolds with RGD did not significantly enhance the performances of the scaffold *in vivo* in terms of cell proliferation and colonization.

Scaffold degradation can be observed after 4 weeks of implantation, as more cracks and holes appeared in both the RGD-free and RGD-modified scaffolds. Due to the swelling of hydrophilic PPE in water and the water solubility of its degradation products, the accumulation of acidic degradation products in tissues *in vivo* is unlikely. These small, water-soluble compounds are expected to be flushed out, so no significant decrease in the local pH is expected. This hypothesis needs to be verified by further *in vivo* experiments, particularly over longer implantation times.

Mason's trichrome staining was performed to evaluate the deposition of extracellular matrix (ECM) inside the scaffold (Figure 9). After 1 week, a limited amount of collagen was observed inside the PPE-based implant (Figure 9A), consistent with moderate cell proliferation observed at this stage of the experiment. In contrast, after 4 weeks, an extensive amount of collagen was clearly visible in the scaffold regions colonized by cells (Figure 9B). Individual collagen fibers were even observed spanning multiple cavities, confirming the ability of the scaffold to serve as support for ECM deposition. In terms of ECM deposition, no significant difference was observed between the RGD-functionalized and bare scaffolds (Figure S7).

The ability of the RDG-grafted scaffolds to support angiogenesis was evaluated by CD31 staining. Although no vascular structures were seen in the PPE scaffold after 1 week (Figure 10A), capillaries ranging from 7 to 30 μm were visible at 4 weeks postimplantation (Figure 10B). Here too, no differences were observed between RGD-grafted scaffolds and naked scaffolds (Figure S8). With this staining, the scaffold can be clearly seen in dark blue on both images (after 1 and 4 weeks), still showing the presence of well-defined circular cavities. Nevertheless, the thickness of the cavity walls decreased after 4 weeks, which further demonstrated the *in vivo* progressive scaffold degradation.

The extent of immune cell infiltration was assessed by CD45 staining, a well-known marker of hematopoietic stem cells.[46] After 1 week, the majority of the cells that started to colonize the RGD-modified scaffold were leukocytes, which is typical of an acute foreign body reaction following implantation (Figure 11A). At 4 weeks postimplantation, leukocytes were still present inside the scaffold, but the surrounding tissues did not show any sign of inflammation (Figure 11B). The inflammatory response was also estimated by counting the percentage of positive pixels exclusively inside the scaffold with QuPath. The percentage of positive pixels significantly increased between the first- and fourth-week postimplantation in both conditions, and the positive surface was higher at 1 week for the nongrafted scaffolds compared to the RDG ones (Figures 12 and S9).

Even though the scaffolds were rapidly colonized by host cells, primarily inflammatory cells were observed, as anticipated based on previous studies.[47,48] A longer implantation period might be required for full acceptance of foreign material by the host animal. However, *in vivo* studies over longer time scales were beyond the scope of the present study.

4. CONCLUSIONS

The present study demonstrates the potential and interest of innovative porous polyphosphoester scaffolds in tissue engineering and regenerative medicine. In this study, for the

https://doi.org/10.1021/acs.biomac.4c01740
Biomacromolecules 2025, 26, 1935−1947

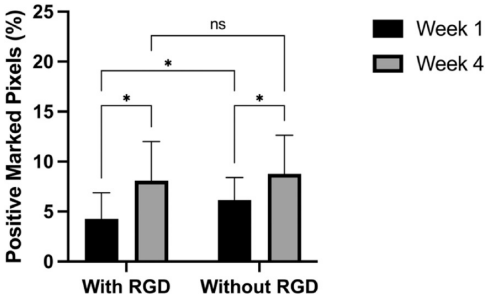


Figure 12. Percentage of CD45 marked pixels inside the RGD-modified and unmodified PPE polyHIPE scaffold after 1 and 4 weeks to evaluate the level of inflammation.

first time, we have shown that the emulsion templating polymerization technology is a very promising strategy to produce interconnected polyphosphoester scaffolds for cell culture and tissue engineering applications. We demonstrated the versatility and tunability of our system by modulating the pore and window sizes as well as the openness of the resulting materials by simply adjusting the surfactant concentration and the volume ratio. The highest pore size (approximately 20 μm) and interconnectivity were obtained using a very low concentration of surfactant (1.25 wt %) in the aqueous phase. Increasing the O/W ratio from 75/25 to 90/10 significantly improved the openness of the scaffold from 0.18 to 0.36. As demonstrated by the *in vitro* and *in vivo* experiments, such porous morphology allowed colonization of the implant by exogenous therapeutic stem cells or endogenous host cells. Pore size could notably be enlarged by decreasing the shearing rate or by using other surfactants in order to further facilitate cell penetration in the scaffold. In their hydrated state, these PPE-based scaffolds exhibited compressive Young's moduli ranging from 3 to 42 kPa, which makes them particularly suitable for soft tissue regeneration applications in organs with inherently low stiffness, such as brain (1−3 kPa), dermis (35 kPa) and hypodermis (2 kPa), pancreas (2.9 kPa), liver (4−6.5 kPa), and muscles (5−170 kPa), to name a few.[37] In this respect, PPE-based polyHIPE scaffolds appear entirely complementary to their polyester-based counterparts that are particularly suited to hard tissue, including bone regeneration. We also showed that the hydrophilic PMEP-based polyHIPE porous scaffold kept its integrity for 1 week of subcutaneous implantation in mice but started to degrade after 4 weeks, as evidenced by the thinning and partial disappearance of the cavity walls. This allowed for a progressive resorption of the scaffold to the benefit of cell invasion. Advantageously, the degradation rate of these PPEs can be tuned by adapting the phosphoester moiety and the side chain, which opens up unique opportunities for adjusting the degradation rate according to the growth rate of the targeted tissues. Finally, direct and indirect toxicity tests performed on stem cells of the apical papilla demonstrated excellent cell viability and so good cytocompatibility of the PPE scaffolds, even when in close contact with cells. PPE scaffolds were then seeded with SCAP, and we confirmed their cytocompatibility, but we also emphasized limited cell adhesion, which was improved via RGD functionalization of the PPE scaffolds. The suitability of the PPE polyHIPES scaffolds for TE applications was confirmed by an in vivo biocompatibility study. Indeed, despite expected inflammatory cell infiltration classically observed after the implantation of any foreign body, the biocompatibility of the scaffolds was confirmed by extensive colonization by host cells and early angiogenesis. Altogether, this study unveils the great potential of PPE scaffolds for tissue engineering applications and paves the way for promising prospects for regenerative medicine.

■ ASSOCIATED CONTENT

Supporting Information

The Supporting Information is available free of charge at https://pubs.acs.org/doi/10.1021/acs.biomac.4c01740.

Detailed formulation of the polyHIPEs, reaction scheme, NMR analysis, SEM analysis, compression modulus, CLSM images, and histological and immunohistological staining (PDF)

■ AUTHOR INFORMATION

Corresponding Authors

Anne des Rieux − *Advanced Drug Delivery and Biomaterials UCLouvain, Université Catholique de Louvain, Louvain Drug Research Institute, 1200 Bruxelles, Belgium;* orcid.org/0000-0001-9953-3816; Email: anne.desrieux@uclouvain.be

Christine Jérôme − *Center for Education and Research on Macromolecules (CERM), PolyHealth Unit, CESAM Research Unit, University of Liège (ULiege), B-4000 Liège, Belgium;* orcid.org/0000-0001-8442-5740; Email: c.jerome@uliege.be

Antoine Debuigne − *Center for Education and Research on Macromolecules (CERM), PolyHealth Unit, CESAM Research Unit, University of Liège (ULiege), B-4000 Liège, Belgium;* orcid.org/0000-0002-7909-7006; Email: adebuigne@uliege.be

Authors

Pascal Boucq − *Center for Education and Research on Macromolecules (CERM), PolyHealth Unit, CESAM Research Unit, University of Liège (ULiege), B-4000 Liège, Belgium*

Bernard Ucakar − *Advanced Drug Delivery and Biomaterials UCLouvain, Université Catholique de Louvain, Louvain Drug Research Institute, 1200 Bruxelles, Belgium*

Floriane Debuisson − *Advanced Drug Delivery and Biomaterials UCLouvain, Université Catholique de Louvain, Louvain Drug Research Institute, 1200 Bruxelles, Belgium*

Raphael Riva − *Center for Education and Research on Macromolecules (CERM), PolyHealth Unit, CESAM Research Unit, University of Liège (ULiege), B-4000 Liège, Belgium*

Complete contact information is available at: https://pubs.acs.org/10.1021/acs.biomac.4c01740

Author Contributions

The manuscript was written through contributions of all authors. All authors have given approval to the final version of the manuscript.

Notes

The authors declare no competing financial interest.

■ ACKNOWLEDGMENTS

The authors gratefully acknowledge financial support from the Fonds de la Recherche Scientifique (F.R.S.-FNRS) for the

HIPEPS PDR project. They also thank Caroline Bouzin, Olivier Van Kerk, and Pierre Michel from the 2IP platform (IREC/UCLouvain) for their help with the preparation of the stained histological samples and advice on the analysis of the results.

REFERENCES

(1) Ghasemi-Mobarakeh, L. Structural Properties of Scaffolds: Crucial Parameters towards Stem Cells Differentiation. *World J. Stem Cells* **2015**, *7* (4), 728.
(2) Steinbach, T.; Wurm, F. R. Poly(Phosphoester)s: A New Platform for Degradable Polymers. *Angew. Chem., Int. Ed.* **2015**, *54* (21), 6098−6108.
(3) Rheinberger, T.; Rabaux, O.; Jérôme, C.; Wurm, F. R. The Future of Polyphosphoesters. *Eur. Polym. J.* **2023**, *200*, No. 112464.
(4) Rheinberger, T.; Deuker, M.; Wurm, F. R. The Microstructure of Polyphosphoesters Controls Polymer Hydrolysis Kinetics from Minutes to Years. *Eur. Polym. J.* **2023**, *190*, No. 111999.
(5) Nifant'ev, I.; Shlyakhtin, A.; Komarov, P.; Tavtorkin, A.; Kananykhina, E.; Elchaninov, A.; Vishnyakova, P.; Fatkhudinov, T.; Ivchenko, P. In Vitro and In Vivo Studies of Biodegradability and Biocompatibility of Poly(ECL)-b-Poly(EtOEP)-Based Films. *Polymers* **2020**, *12* (12), No. 3039.
(6) Li, Q.; Wang, J.; Shahani, S.; Sun, D. D. N.; Sharma, B.; Elisseeff, J. H.; Leong, K. W. Biodegradable and Photocrosslinkable Polyphosphoester Hydrogel. *Biomaterials* **2006**, *27* (7), 1027−1034.
(7) Qiu, J.; Liu, C.; Hu, F.; Guo, X.; Zheng, Q. Synthesis of Unsaturated Polyphosphoester as a Potential Injectable Tissue Engineering Scaffold Materials. *J. Appl. Polym. Sci.* **2006**, *102* (4), 3095−3101.
(8) Riva, R.; Shah, U.; Thomassin, J.-M.; Yilmaz, Z.; Lecat, A.; Colige, A.; Jérôme, C. Design of Degradable Polyphosphoester Networks with Tailor-Made Stiffness and Hydrophilicity as Scaffolds for Tissue Engineering. *Biomacromolecules* **2020**, *21* (2), 349−355.
(9) Pelosi, C.; Tinè, M. R.; Wurm, F. R. Main-Chain Water-Soluble Polyphosphoesters: Multi-Functional Polymers as Degradable PEG-Alternatives for Biomedical Applications. *Eur. Polym. J.* **2020**, *141*, No. 110079.
(10) Yilmaz, Z. E.; Jérôme, C. Polyphosphoesters: New Trends in Synthesis and Drug Delivery Applications. *Macromol. Biosci.* **2016**, *16* (12), 1745−1761.
(11) Yang, X.-Z.; Sun, T.-M.; Dou, S.; Wu, J.; Wang, Y.-C.; Wang, J. Block Copolymer of Polyphosphoester and Poly(l-Lactic Acid) Modified Surface for Enhancing Osteoblast Adhesion, Proliferation, and Function. *Biomacromolecules* **2009**, *10* (8), 2213−2220.
(12) Iwasaki, Y. Bone Mineral Affinity of Polyphosphodiesters. *Molecules* **2020**, *25*, 758.
(13) Otaka, A.; Kiyono, K.; Iwasaki, Y. Enhancement of Osteoblast Differentiation Using Poly(Ethylene Sodium Phosphate). *Materialia* **2021**, *15*, No. 100977.
(14) Hao, Y.; He, J.; Ma, X.; Feng, L.; Zhu, M.; Zhai, Y.; Liu, Y.; Ni, P.; Cheng, G. A Fully Degradable and Photocrosslinked Polysaccharide-Polyphosphate Hydrogel for Tissue Engineering. *Carbohydr. Polym.* **2019**, *225*, No. 115257.
(15) Wachiralarpphaithoon, C.; Iwasaki, Y.; Akiyoshi, K. Enzyme-Degradable Phosphorylcholine Porous Hydrogels Cross-Linked with Polyphosphoesters for Cell Matrices. *Biomaterials* **2007**, *28* (6), 984−993.
(16) Karageorgiou, V.; Kaplan, D. Porosity of 3D Biomaterial Scaffolds and Osteogenesis. *Biomaterials* **2005**, *26* (27), 5474−5491.
(17) Aldemir Dikici, B.; Claeyssens, F. Basic Principles of Emulsion Templating and Its Use as an Emerging Manufacturing Method of Tissue Engineering Scaffolds. *Front. Bioeng. Biotechnol.* **2020**, *8*, No. 875, DOI: 10.3389/fbioe.2020.00875.
(18) Owen, R.; Sherborne, C.; Paterson, T.; Green, N. H.; Reilly, G. C.; Claeyssens, F. Emulsion Templated Scaffolds with Tunable Mechanical Properties for Bone Tissue Engineering. *J. Mech. Behav. Biomed. Mater.* **2016**, *54*, 159−172.
(19) Zhang, T.; Sanguramath, R. A.; Israel, S.; Silverstein, M. S. Emulsion Templating: Porous Polymers and Beyond. *Macromolecules* **2019**, *52* (15), 5445−5479.
(20) Foudazi, R. HIPEs to PolyHIPEs. *React. Funct. Polym.* **2021**, *164*, No. 104917.
(21) Kramer, S.; Cameron, N. R.; Krajnc, P. Porous Polymers from High Internal Phase Emulsions as Scaffolds for Biological Applications. *Polymers* **2021**, *13* (11), 1786.
(22) Silverstein, M. S. Emulsion-Templated Polymers: Contemporary Contemplations. *Polymer* **2017**, *126*, 261−282.
(23) Onder, O. C.; Utroša, P.; Caserman, S.; Podobnik, M.; Žnidarič, M. T.; Grdadolnik, J.; Kovačič, S.; Žagar, E.; Pahovnik, D. Emulsion-Templated Synthetic Polypeptide Scaffolds Prepared by Ring-Opening Polymerization of *N* -Carboxyanhydrides. *Polym. Chem.* **2020**, *11* (26), 4260−4270.
(24) Kapilov-Buchman, K.; Bialystocki, T.; Niezni, D.; Perry, L.; Levenberg, S.; Silverstein, M. S. Porous Polycaprolactone and Polycarbonate Poly(Urethane Urea)s *via* Emulsion Templating: Structures, Properties, Cell Growth. *Polym. Chem.* **2021**, *12* (45), 6569−6581.
(25) Aldemir Dikici, B.; Sherborne, C.; Reilly, G. C.; Claeyssens, F. Emulsion Templated Scaffolds Manufactured from Photocurable Polycaprolactone. *Polymer* **2019**, *175*, 243−254.
(26) Jackson, C. E.; Ramos-Rodriguez, D. H.; Farr, N. T. H.; English, W. R.; Green, N. H.; Claeyssens, F. Development of PCL PolyHIPE Substrates for 3D Breast Cancer Cell Culture. *Bioengineering* **2023**, *10* (5), 522.
(27) Aldemir Dikici, B.; Malayeri, A.; Sherborne, C.; Dikici, S.; Paterson, T.; Dew, L.; Hatton, P.; Ortega Asencio, I.; MacNeil, S.; Langford, C.; Cameron, N. R.; Claeyssens, F. Thiolene-and Polycaprolactone Methacrylate-Based Polymerized High Internal Phase Emulsion (PolyHIPE) Scaffolds for Tissue Engineering. *Biomacromolecules* **2022**, *23* (3), 720−730.
(28) Aldemir Dikici, B.; Reilly, G. C.; Claeyssens, F. Boosting the Osteogenic and Angiogenic Performance of Multiscale Porous Polycaprolactone Scaffolds by *In Vitro* Generated Extracellular Matrix Decoration. *ACS Appl. Mater. Interfaces* **2020**, *12* (11), 12510−12524.
(29) Aldemir Dikici, B.; Chen, M.-C.; Dikici, S.; Chiu, H.-C.; Claeyssens, F. *In Vivo* Bone Regeneration Capacity of Multiscale Porous Polycaprolactone-Based High Internal Phase Emulsion (PolyHIPE) Scaffolds in a Rat Calvarial Defect Model. *ACS Appl. Mater. Interfaces* **2023**, *15* (23), 27696−27705.
(30) Pratt, R. C.; Lohmeijer, B. G. G.; Long, D. A.; Lundberg, P. N. P.; Dove, A. P.; Li, H.; Wade, C. G.; Waymouth, R. M.; Hedrick, J. L. Exploration, Optimization, and Application of Supramolecular Thiourea−Amine Catalysts for the Synthesis of Lactide (Co)-Polymers. *Macromolecules* **2006**, *39* (23), 7863−7871.
(31) Thijssen, Q.; Parmentier, L.; Van holsbeeck, K.; Ballet, S.; Van Vlierberghe, S. Nature-Inspired Dual Purpose Strategy toward Cell-Adhesive PCL Networks: C(-Linker-)RGD Incorporation via Thiol-Ene Crosslinking. *Biomacromolecules* **2023**, *24* (4), 1638−1647.
(32) Ruparel, N. B.; de Almeida, J. F. A.; Henry, M. A.; Diogenes, A. Characterization of a Stem Cell of Apical Papilla Cell Line: Effect of Passage on Cellular Phenotype. *J. Endod.* **2013**, *39* (3), 357−363.
(33) Lizcano-Perret, B.; Lardinois, C.; Wavreil, F.; Hauchamps, P.; Herinckx, G.; Sorgeloos, F.; Vertommen, D.; Gatto, L.; Michiels, T. Cardiovirus Leader Proteins Retarget RSK Kinases toward Alternative Substrates to Perturb Nucleocytoplasmic Traffic. *PLoS Pathog.* **2022**, *18* (12), No. e1011042.
(34) Choteau, M.; Scohy, A.; Messe, S.; Luyckx, M.; Dechamps, M.; Montiel, V.; Yombi, J. C.; Gruson, D.; Limaye, N.; Michiels, T.; Dumoutier, L. Development of SARS-CoV2 Humoral Response Including Neutralizing Antibodies Is Not Sufficient to Protect Patients against Fatal Infection. *Sci. Rep.* **2022**, *12* (1), No. 2077.
(35) Tee, H. T.; Zipp, R.; Koynov, K.; Tremel, W.; Wurm, F. R. Poly(Methyl Ethylene Phosphate) Hydrogels: Degradable and Cell-Repellent Alternatives to PEG-Hydrogels. *Eur. Polym. J.* **2020**, *141*. 110075.

https://doi.org/10.1021/acs.biomac.4c01740
Biomacromolecules 2025, 26, 1935−1947

(36) Ruckenstein, E. Microemulsions, Macroemulsions, and the Bancroft Rule. *Langmuir* **1996**, *12* (26), 6351−6353.
(37) Xu, H.; Casillas, J.; Krishnamoorthy, S.; Xu, C. Effects of Irgacure 2959 and Lithium Phenyl-2,4,6-Trimethylbenzoylphosphinate on Cell Viability, Physical Properties, and Microstructure in 3D Bioprinting of Vascular-like Constructs. *Biomed. Mater.* **2020**, *15* (5), No. 055021.
(38) Zhang, S.; Chen, M.; You, Y.; Wang, Y.; Zhu, Y. Mechanism of Interconnected Pore Formation in High Internal Phase Emulsion-Templated Polymer. *ACS Macro Lett.* **2024**, *13* (8), 903−907.
(39) Guimarães, C. F.; Gasperini, L.; Marques, A. P.; Reis, R. L. The Stiffness of Living Tissues and Its Implications for Tissue Engineering. *Nat. Rev. Mater.* **2020**, *5* (5), 351−370.
(40) Liu, J.; Zheng, H.; Poh, P.; Machens, H.-G.; Schilling, A. Hydrogels for Engineering of Perfusable Vascular Networks. *Int. J. Mol. Sci.* **2015**, *16* (7), 15997−16016.
(41) Handorf, A. M.; Zhou, Y.; Halanski, M. A.; Li, W.-J. Tissue Stiffness Dictates Development, Homeostasis, and Disease Progression. *Organogenesis* **2015**, *11* (1), 1−15.
(42) Chitrakar, C.; Hedrick, E.; Adegoke, L.; Ecker, M. Flexible and Stretchable Bioelectronics. *Materials* **2022**, *15* (5), 1664.
(43) Bauer, K. N.; Liu, L.; Wagner, M.; Andrienko, D.; Wurm, F. R. Mechanistic Study on the Hydrolytic Degradation of Polyphosphates. *Eur. Polym. J.* **2018**, *108*, 286−294.
(44) Pérez, M. B.; Resendiz-Lara, D. A.; Matsushita, Y.; Kakinoki, S.; Iwasaki, Y.; Hempenius, M. A.; de Beer, S.; Wurm, F. R. Creating Anti-Biofouling Surfaces by Degradable Main-chain Polyphosphoester Polymer Brushes. *Adv. Funct. Mater.* **2024**, *34* (32), No. 2316201, DOI: 10.1002/adfm.202316201.
(45) Hersel, U.; Dahmen, C.; Kessler, H. RGD Modified Polymers: Biomaterials for Stimulated Cell Adhesion and Beyond. *Biomaterials* **2003**, *24* (24), 4385−4415.
(46) Zheng, S.; Epstein, P. CD45 Immunohistochemistry in Mouse Kidney. *Bio-Protoc.* **2021**, *11* (22), No. e4230, DOI: 10.21769/BioProtoc.4230.
(47) Anderson, J. M.; Rodriguez, A.; Chang, D. T. Foreign Body Reaction to Biomaterials. *Semin. Immunol.* **2008**, *20* (2), 86−100.
(48) Modulevsky, D. J.; Cuerrier, C. M.; Pelling, A. E. Biocompatibility of Subcutaneously Implanted Plant-Derived Cellulose Biomaterials. *PLoS One* **2016**, *11* (6), No. e0157894.

https://doi.org/10.1021/acs.biomac.4c01740
Biomacromolecules 2025, 26, 1935−1947